Available online at www.sciencedirect.com
SCIENCE DIRECT®
International Journal of Heat and Mass Transfer 49 (2006) 3866–3878
International Journal of HEAT and MASS TRANSFER
www.elsevier.com/locate/ijhmt

Numerical prediction of a two-phase fluid driving system using cavitating flow of magnetic fluid

Jun Ishimoto *

Institute of Fluid Science, TFI Research Center, Tohoku University, 2-1-1, Katahira, Aoba-ku, Sendai 980-8577, Japan

Received 6 October 2005
Available online 27 June 2006

Abstract

A new concept of a two-phase fluid driving system using cavitating flow of a magnetic fluid is proposed, and the driving and acceleration performance of the system is numerically predicted. A typical computational model for cavitating flow of a magnetic fluid is proposed and several flow characteristics, taking into account the strong nonuniform magnetic field, are numerically investigated to realize the further development and high performance of the proposed new type of two-phase fluid driving system using magnetic fluids. Based on numerical results, the two-dimensional structure of the cavitating flow as well as the cloud cavity formation of the magnetic fluid through a vertical converging–diverging channel are shown in detail. The numerical results demonstrate that an effective two-phase magnetic driving force and fluid acceleration can be obtained by the practical use of magnetization of the working fluid. Also clarified is the cavitation number in the case of a strong magnetic field with a larger value than that in the case of a nonmagnetic field. Magnetic control for suppression of cavitation bubbles is remarkably enhanced in the condition of high Reynolds number. Further clarified is the precise control of the cavitating flow of magnetic fluid that is possible by effective use of the magnetic body force that acts on cavitation bubbles.

PACS: 47.55.Kf; 47.55.Bx; 47.65.+a

Keywords: Magnetic fluid; Multiphase flow; Cavitation; Magnetohydrodynamics; Liquid metal MHD; Internal flow

1. Introduction

Magnetic fluids are a colloidal suspension of many fine particles of a solid magnetic material (mean diameter $\approx$10 nm, number density $\approx 10^{23}/m^3$) in a carrier liquid such as water, hydrocarbon, ester and fluorocarbon. The particles are usually stabilized to overcome magnetic and van der Waals interactions by coating the particles with a surfactant. A most interesting feature is to the liquid that can respond to magnetic field. This characteristics result from the magnetic stress (Maxwell's stress) occurring in a magnetic field. The precise investigation for the cavitation and two-phase flow phenomena of magnetic fluid is very interesting and important not only as basic study on hydrodynamics of magnetic fluids, but also for finding solutions to problems related to the development of practical engineering applications of magnetic fluids, such as the new energy conversion system using two-phase flows of magnetic fluid which has been proposed by the author [1,2].

The principle of such a fluid driving system is schematically depicted in Fig. 1. In this system, the flow is accelerated in the region of the converging nozzle, and cavitation inception is induced at a point downstream of the throat of a diverging nozzle due to a pressure decrease. Furthermore, the flow is additionally accelerated not only by the pumping effect of the cavitation bubbles, but also by the rise of magnetic pressure induced by the unbalance of magnetic body forces in the single- and two-phase flow regions under a nonuniform magnetic field. The idea of using a two-phase flow system originated from the two-phase liquid–metal

* Tel./fax: +81 22 217 5271.
E-mail address: ishimotojun@ieee.org
URL: http://alba.ifs.tohoku.ac.jp/

0017-9310/$ - see front matter © 2006 Elsevier Ltd. All rights reserved.
doi:10.1016/j.ijheatmasstransfer.2006.04.023

Nomenclature

$a^{(i)}$	interfacial area concentration per unit volume
C_D	drag coefficient
C_V	virtual mass coefficient
c_p	specific heat at constant pressure
c_0	sound velocity
D	inlet width of duct
e	specific internal energy
e^{ijk}	permutation symbol
g_r^i	contravariant vector of gravitational acceleration
g^{ij}	fundamental metric tensor
H	strength of magnetic field
H^i	contravariant vector of magnetic field
H_{max}	maximum strength of magnetic field
h	specific enthalpy
k	heat transfer rate
k_B	Boltzmann's constant
M	strength of magnetization
M^i	contravariant vector of magnetization
N	number density
p	absolute pressure
q	heat flux
q^i	contravariant heat flux vector
R	radius
$\Re$	gas constant
T	absolute temperature
T_s	saturation temperature
t	time
u^i, u^j, u^k	contravariant velocity
u_i, u_j, u_k	covariant velocity

Greek symbols

α	volume fraction
β	dynamic viscosity
Γ	phase generation density
γ	surface tension
η	transverse coordinate
κ	ratio of specific heat
λ	thermal conductivity
μ_0	magnetic permeability in vacuum
ν	kinematic viscosity
ξ	longitudinal coordinate
ρ	density
Ω^i	contravariant angular velocity vector
ω^i	contravariant vorticity vector
∇_j	covariant differential

Subscripts and superscripts

$()_c$	condensation
$()_e$	evaporation
$()_{(ex)}$	exit section of the duct
$()_g$	gas phase
$()^i, ()^j, ()^k$	contravariant component
$()_i, ()_j, ()_k$	covariant component
$()^{(i)}$	interface
$()_{(in)}$	inlet section of the duct
$()_l$	liquid phase
$()_s$	saturation
$()_T$	two-phase
$()_{(th)}$	nozzle throat
$()^{\xi}$	contravariant component in the ξ-direction
$()^{\eta}$	contravariant component in the η-direction
$\overline{()}$	mean value

MHD power generation system which was proposed and developed by Petrick and Branover [3]. Subsequent to their proposal, we reported the results of a theoretical study which demonstrated the possibility of using an electrically conducting magnetic fluid [4–7] as a working fluid in a liquid–metal MHD power generation system [8]. Our results indicated that a better driving force or pressure rise than that of the conventional system could be obtained by using an electrically conducting magnetic fluid as the working fluid due to the advantage of the practical application of fluid magnetization. According to these previous studies, it is likely that high performance of the power generation system is possible by application of electrically conducting magnetic fluid to the working fluid in the two-phase LMMHD [9,10] power generation system.

In the past few years, theoretical and experimental studies on the basic characteristics of two-phase flow of magnetic fluid have been conducted and the possibility of flow control or effective driving force generation by magnetic force in the new energy conversion system using two-phase flow has been confirmed [1,2]. It has also been concluded that stabilization of two-phase flow is possible by effective application of the magnetic force of the fluid [2,11]. In the application of two-phase flow of magnetic fluid to an actual fluid transport apparatus, it is important to determine a simple and effective method to generate a two-phase flow state so as to improve the total performance of a fluid driving system using multiphase flow.

However, conventional two-phase flow systems essentially require a powerful heat source or gas-injection equipment for generation of a boiling two-phase flow or a gas–liquid two-phase flow state. Additionally, research on methods for the production of the two-phase magnetic fluid flow state have not been precisely focused, and only a few studies have so far been made on the basic mechanism of cavitating flow due to the difficulty of confirming

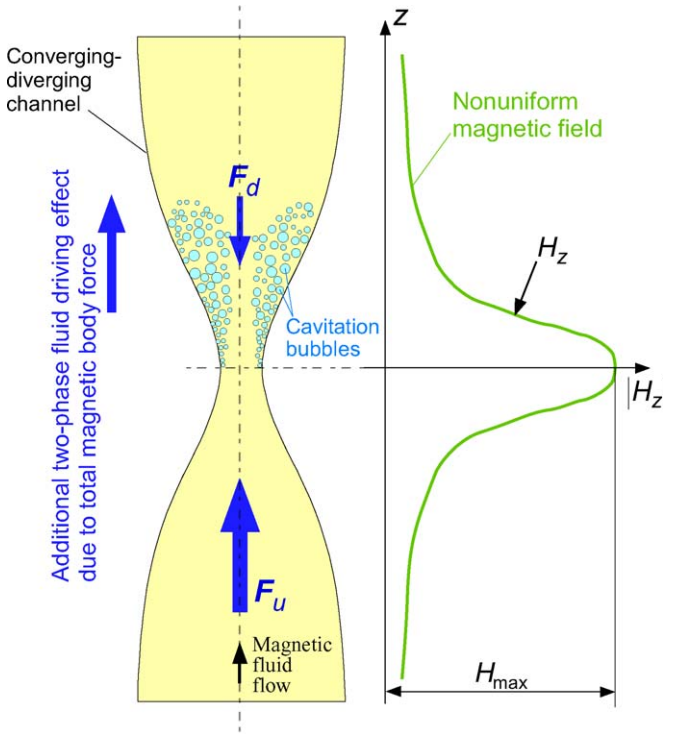

Fig. 1. Principle of two-phase fluid driving system using cavitating flow of magnetic fluid. Magnetic body force $\boldsymbol{F}_u = \mu_0 \boldsymbol{M} \cdot \nabla \boldsymbol{H} = \boldsymbol{F}_d$ in the case without cavitation, and $\boldsymbol{F}_d = (1 - \alpha_g)\mu_0 \boldsymbol{M} \cdot \nabla \boldsymbol{H} < \boldsymbol{F}_u$ with cavitation ($\boldsymbol{H}$ is the vector of magnetic field and $\boldsymbol{M}$ is the vector of magnetization).

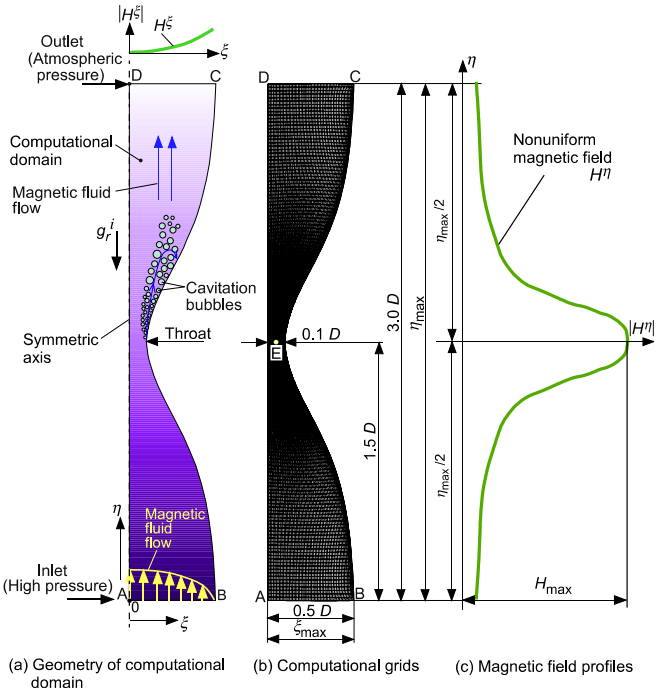

Fig. 2. Schematic of computational system used in numerical analysis.

experimental and theoretical results in high-speed two-phase magnetic fluid flow with phase change. To overcome these difficulties, we contrived a new type of two-phase fluid driving and acceleration system by using cavitating flow of magnetic fluid. A prominent feature of this system is that there are no heat sources nor additional gas-injection devices except for a converging–diverging nozzle. Based on an advanced mathematical model, which takes the effect of two-phase magnetic body force acting on the cavitating magnetic fluid flow state into consideration, we developed a new method for analyzing cavitating flow.

In the present study, two-dimensional characteristics of cavitating flow of magnetic fluid in a converging–diverging channel with phase change are numerically investigated to facilitate the further development and high performance of a two-phase fluid acceleration system or fluid transport applications. First, the governing equations of cavitating flow of magnetic fluid based on the unsteady two-fluid model in the generalized curvilinear coordinates system are presented, and then several cavitating flow characteristics are numerically calculated, taking into account the effect of the strong nonuniform magnetic field.

2. Numerical method

2.1. Governing equations

The system used in the numerical analysis is schematically depicted in Fig. 2. In the initial stationary state, the flow duct is filled with pressurized hexane-based magnetic fluid, and flow immediately occurs when the outlet D–C is opened. Magnetic fluid is continuously introduced with high-speed via the inlet section A–B, the flow is accelerated at the point of the converging–diverging nozzle, and the inception of cavitation is induced by a pressure decrease.

In the present numerical formulation of the cavitating flow characteristics of magnetic fluid, we extend the general two-fluid model to a vapor–liquid multiphase fluid taking into account the effect of strong nonuniform magnetic field for analysis, which is based on the unsteady thermal non-equilibrium two-fluid model of Kataoka [12], and Harlow and Amsden [13]. In the numerical model, the condition of the working fluid with the cavitating magnetic fluid flow structure can be approximated to form a homogeneously dispersed bubbly flow because the physical properties such as latent heat for vaporization, density, viscosity, and surface tension of the hexane-based magnetic fluid are very small compared with those of pure water at room temperature. Accordingly, it seems reasonable to assume that a cavitating flow pattern is easily formed in the bubbly two-phase flow. In the process of modeling, to consider the effects of the rapid evaporation and condensation of magnetic fluid, we apply the rapid phase-change model of Yamamoto et al. [14] and Young [15] to the cavitating flow of magnetic fluid.

The calculation is carried out using the two-dimensional generalized curvilinear coordinate system (ξ, η) as shown in Fig. 2; ξ and η denote the transverse and longitudinal coordinates, respectively. The model for analysis simulates the cavitating flow of magnetic fluid passing through a converging–diverging channel in a vertical duct. It is assumed

that the flow field is symmetric to the central axis D–A as shown in Fig. 2. A nonuniform magnetic field is applied in the longitudinal η-direction, which is parallel to the mainstream of working fluid flow. In the numerical modeling under this condition, the following assumptions are employed to formulate the governing equations:

(1) The cavitating flow is a two-dimensional unsteady internal flow.
(2) The magnetic field is not influenced by the existence of the gas phase.
(3) The applied magnetic field is homogeneous and steady.
(4) The energy exchange between the liquid and gas phases is taken into account.
(5) The liquid phase is incompressible fluid.

According to the previous study on single bubble in magnetic fluid [16], it has been found that the effect of bubbles existence on magnetic field is revealed in the limited condition of the large bubble diameter in the order of 3.0–5.0 mm. It is found that the bubble deforms and is elongated in the direction of magnetic field because of the inhomogeneous magnetic pressure distribution at the interface between the gas- and the liquid phases. The nonuniformity of magnetic pressure is caused by the transient deformation of the magnetic field with refraction of magnetic flux at the interface due to the difference of magnetic susceptibility between the paramagnetic liquid phase and the almost diamagnetic gas phase. The bubble diameter which deal with the present analysis, the cavitation bubble expands maximum to the small diameter of about 0.50 mm under the strong magnetic field. In that small diameter condition, the surface tension at the interface is more dominant than the magnetic deformation force at there. Therefore, the influence of magnetic field on bubbles is neglected in the present analysis. Under the above conditions, the governing equations of the cavitating magnetic fluid flow, taking into account the effect of nonuniform magnetic field based on the unsteady two-dimensional two-fluid model, are derived as follows.

The mass conservation equation for the gas and liquid phases is

$$\frac{\partial}{\partial t}(\alpha_m \rho_m) + \nabla_j(\alpha_m \rho_m u_m^j) = \Gamma_m, \tag{1}$$

where the subscript m denotes the gas phase ($m = \mathrm{g}$) or liquid phase ($m = \mathrm{l}$). t is the time, α_g and α_l are the gas- and liquid-phase volume fraction, respectively, ρ_g and ρ_l are the gas- and liquid-phase densities, respectively. The relationship ($\alpha_\mathrm{g} + \alpha_\mathrm{l} = 1$) is assumed. u_g^j and u_l^j are the gas- and liquid-phase contravariant velocities, respectively, Γ_g and Γ_l are the gas- and liquid-phase generation densities, respectively, and ∇_j is the covariant differential. The superscripts and subscripts (i,j,k) denote the contravariant and covariant components, respectively.

The combined equation of motion for the total gas and liquid phase is

$$\begin{aligned}\frac{\partial}{\partial t}(\alpha_\mathrm{g}\rho_\mathrm{g}u_\mathrm{g}^i + \alpha_\mathrm{l}\rho_\mathrm{l}u_\mathrm{l}^i) + \nabla_j(\alpha_\mathrm{g}\rho_\mathrm{g}u_\mathrm{g}^i u_\mathrm{g}^j + \alpha_\mathrm{l}\rho_\mathrm{l}u_\mathrm{l}^i u_\mathrm{l}^j)\\ = -g^{ij}\nabla_j p_\mathrm{l} + \mu_0\alpha_\mathrm{l}M^j\nabla_j H^i + g^{jk}\nabla_j\nabla_k\beta_\mathrm{T}u_\mathrm{l}^i\\ + g^{ik}\nabla_j\nabla_k\beta_\mathrm{T}u_\mathrm{l}^j - \frac{2}{3}(\nabla_j\nabla_k\beta_\mathrm{T}u_\mathrm{l}^k)g^{ij} + (\alpha_\mathrm{g}\rho_\mathrm{g} + \alpha_\mathrm{l}\rho_\mathrm{l})g_r^i,\end{aligned} \tag{2}$$

where the second term of the right-hand side of Eq. (2) represents the magnetic body force term in two-phase flow, H^i is the contravariant vector of the magnetic field, M^j is the contravariant vector of the magnetization, g^{ij} is the fundamental metric tensor, p is the absolute pressure, μ_0 is the permeability in vacuum, and g_r^i is the contravariant vector of gravitational acceleration.

Additionally, β_T in Eq. (2) denotes the viscosity of the two-phase mixture flow that includes small dispersed bubbles. β_T was evaluated using the following formula for the viscosity of a suspension [17–19]:

$$\beta_\mathrm{T} = \left[1 - \left(\frac{\alpha_\mathrm{g}}{0.680}\right)\right]^{-2} \cdot \beta_\mathrm{l} \quad (\alpha_\mathrm{g} < 0.5). \tag{3}$$

To consider the effects of additional forces that act on the bubbles and the effects of radial expansion of the bubbles, the equation of motion for the gas phase is here replaced with the translational motion of a single bubble [20]. Therefore, the Eulerian–Lagrangian two-way coupling model [21,22] is applied to predict the two-dimensional cavitating flow characteristics.

The equation of motion for the gas phase is

$$\frac{4}{3}\pi\rho_\mathrm{g}R_\mathrm{g}^3\frac{\mathrm{d}u_\mathrm{g}^i}{\mathrm{d}t} = -F_p^i + F_g^i - F_\mathrm{D}^i - F_\mathrm{VM}^i - F_\mathrm{B}^i + F_\mathrm{LM}^i + F_\mathrm{LS}^i, \tag{4}$$

where each additional force term is derived as follows:

$$F_p^i = \frac{4}{3}\pi R_\mathrm{g}^3 g^{ij}\nabla_j p_\mathrm{l} \tag{5}$$

$$F_g^i = \frac{4}{3}\pi R_\mathrm{g}^3\rho_\mathrm{g}g_r^i \tag{6}$$

$$F_\mathrm{D}^i = \frac{1}{2}\rho_\mathrm{l}C_\mathrm{D}|u_\mathrm{g}^i - u_\mathrm{l}^i|(u_\mathrm{g}^i - u_\mathrm{l}^i)\pi R_\mathrm{g}^2 \tag{7}$$

$$F_\mathrm{VM}^i = C_\mathrm{VM}\cdot\rho_\mathrm{l}\frac{4}{3}\pi R_\mathrm{g}^3\left[\frac{\mathrm{d}}{\mathrm{d}t}(u_\mathrm{g}^i - u_\mathrm{l}^i) + \frac{3}{R_\mathrm{g}}(u_\mathrm{g}^i - u_\mathrm{l}^i)\frac{\mathrm{d}R_\mathrm{g}}{\mathrm{d}t}\right] \tag{8}$$

$$F_\mathrm{B}^i = 6R_\mathrm{g}^2\sqrt{\pi\rho_\mathrm{l}\beta_\mathrm{l}}\int_0^t \frac{\frac{\mathrm{d}}{\mathrm{d}\tau}(u_\mathrm{g}^i - u_\mathrm{l}^i)}{\sqrt{t-\tau}}\mathrm{d}\tau \tag{9}$$

$$F_\mathrm{LM}^i = \pi R_\mathrm{g}^3\rho_\mathrm{l}\mathrm{e}^{ijk}(\Omega_{\mathrm{g}j} - \Omega_{\mathrm{l}j})(u_{\mathrm{g}k} - u_{\mathrm{l}k}) \tag{10}$$

$$F_\mathrm{LS}^i = 6.46\frac{\beta_\mathrm{l}R_\mathrm{g}^2}{\sqrt{|(\Omega_\mathrm{g}^i - \Omega_\mathrm{l}^i)|\nu_\mathrm{l}}}\mathrm{e}^{ijk}(\Omega_{\mathrm{g}j} - \Omega_{\mathrm{l}j})(u_{\mathrm{g}k} - u_{\mathrm{l}k}) \tag{11}$$

$$\Omega_\mathrm{l}^i = \frac{1}{2}\omega_\mathrm{l}^i = \frac{1}{4}\mathrm{e}^{ijk}(\nabla_j u_{\mathrm{l}k} - \nabla_k u_{\mathrm{l}j}), \tag{12}$$

where F_p^i is the force due to the liquid-phase pressure gradient, F_g^i is the gravitational acceleration force, F_D^i is the

drag force, F^i_{VM} is the virtual mass force considering the expansion of a bubble, and F^i_B is the Basset history term, which takes into account the effect of the deviation in flow pattern from the steady state. F^i_{LM} is the Magnus lift force caused by the rotation of the bubble as reported by Auton [23]. F^i_{LS} is Saffman's lift force [24] caused by the velocity gradient of the liquid phase. C_D is the drag coefficient, C_{VM} is the virtual mass coefficient, R_g is the equivalent bubble diameter, Ω^i is the contravariant angular velocity, and ω^i is the contravariant vorticity. d/dt denotes the substantial derivative.

The equation for the angular velocity of a bubble is derived as follows [24]:

$$\frac{d\Omega^i_g}{dt} = \frac{15\beta_l}{R_g^2 \cdot \rho_g}(\Omega^i_l - \Omega^i_g). \tag{13}$$

The energy equation for the gas and liquid phases is

$$\begin{aligned}&\frac{\partial}{\partial t}(\alpha_m \rho_m e_m) + \nabla_j(\alpha_m \rho_m e_m u^j_m)\\ &\quad = -p_m \frac{\partial \alpha_m}{\partial t} - \nabla_j(\alpha_m p_m u^j_m) + \Gamma_m h^{(i)}_m + q^{(i)}_m a^{(i)}\\ &\qquad - \nabla_j(\alpha_m q^j_m) + \alpha_m \Phi_m.\end{aligned} \tag{14}$$

In the above equation, the subscript m denotes the gas phase ($m = g$) or liquid phase ($m = l$). $h^{(i)}_g$ and $h^{(i)}_l$ are the enthalpy of the gas phase and that of the liquid phase at the interface, respectively. $a^{(i)}$ is the gas–liquid interfacial area concentration per unit volume. $\Gamma_g h^{(i)}_g$ and $\Gamma_l h^{(i)}_l$ are the interfacial energy transfer terms due to the liquid–vapor phase change. $q^{(i)}_g$ and $q^{(i)}_l$ are the heat transfer terms of mutual interaction between the vapor and liquid interface. q^j is the contravariant heat flow vector, and Φ is the energy dissipation function, as described below:

$$\begin{cases} q^i_m = -\lambda_m g^{ij} \nabla_j T_m, \\ \Phi_m = -\dfrac{2}{3}\beta_m (\nabla_i u^i_m)^2 + 2\beta_m s^i_{jm} s^j_{im}, \\ s^i_{jm} = \dfrac{1}{2}(\nabla_j u^i_m + \nabla_i u^j_m). \end{cases} \tag{15}$$

We assume that the mass of each vapor bubble and that of the condensed liquid droplet in each computational location is constant. Based on this assumption, the mass conservation equation for number density N_k is derived as follow:

$$\frac{\partial}{\partial t}\left(\frac{4}{3}\pi R^3_k N_k \rho_k\right) + \nabla_j\left(\frac{4}{3}\pi R^3_k N_k \rho_k u^j_k\right) = \Gamma_k, \tag{16}$$

$$\begin{cases} k = e: \quad R_k = R_g, \quad N_k = N_g, \quad \rho_k = \rho_g, \quad u^i_k = u^i_g, \quad \Gamma_k = \Gamma_g, \\ k = c: \quad R_k = R_l, \quad N_k = N_l, \quad \rho_k = \rho_l, \quad u^i_k = u^i_l, \quad \Gamma_k = \Gamma_l, \end{cases}$$

where subscript k denotes evaporation ($k = e$) or condensation ($k = c$).

The governing equations of cavitating flow mentioned above are constructed by Eulerian-type equations for the liquid phase and by Lagrangian-type equations for the gas phase.

2.2. Constitutive equations

The drag coefficient (C_D) and the virtual mass coefficient (C_{VM}) are defined as follows [24]:

$$\begin{cases} C_D = \dfrac{24}{Re_B}(1 + 0.15 Re_B^{0.687}) + \dfrac{0.42}{1 + 42,500 Re_B^{-1.16}}, \\ C_{VM} = 0.5, \\ Re_B = \dfrac{\rho_l |u^i_g - u^i_l| D}{\beta_l}. \end{cases} \tag{17}$$

The energy balance condition at the interface of the gas and liquid phases is expressed by the following equation:

$$\begin{cases} \Gamma_g h^{(i)}_g + \Gamma_l h^{(i)}_l = 0, \\ q^{(i)}_g + q^{(i)}_l = 0, \end{cases} \tag{18}$$

where $h_k = c_{pk} T_k$; ($k = g, l$). Detailed constitutive equations for interfacial energy transfer terms in Eq. (18) are given by following extended empirical formulas [25,26]:

$$q^{(i)}_g = k^{(i)}(T_g - T_s), \tag{19}$$

where $k^{(i)}$ is the interfacial heat transfer rate between the gas and liquid phases, which is given by following equations [25]:

$$\begin{cases} k^{(i)} = \alpha k^{(i)}_g + \alpha_l k^{(i)}_l, \\ k^{(i)}_g = \dfrac{8.067 \cdot \lambda_g}{R_g}, \\ k^{(i)}_l = \dfrac{1.0 + 0.37 Re_V^{0.50} \cdot Pr_V^{0.35}}{R_g}, \\ Re_V = \dfrac{2.0 R_g |u^i_g - u^i_l|}{\nu_l}, \\ Pr_V = \dfrac{c_{pl} \cdot \beta_l}{\lambda_l}. \end{cases} \tag{20}$$

It is assumed that the energy transfer is caused by the heat transfer between the isothermal spherical bubbles and the surrounding liquid. Assuming a spherical bubble with equivalent radius R_g, the expression of the interfacial area concentration per unit volume $a^{(i)}$ is obtained by the following equation [12]:

$$a^{(i)} = \frac{3\alpha_g}{R_g}. \tag{21}$$

In general, the interfacial transfer terms are proportional to the interfacial area concentration, $a^{(i)}$. Therefore, $a^{(i)}$ is one of the most important parameters in the two-fluid model. Assuming that the vapor gas phase follows an ideal gas law and that the relationship between gas-phase pressure (p_g) and density (ρ_g) obeys polytropic change, the following equation by Hirt and Romero [27] results:

$$\rho_g(\kappa_g - 1)e_g = [p_g - c^2_{l0}\rho_l(\alpha^*_g - \alpha_g)]\alpha^*_g, \tag{22}$$

$$\begin{cases} \alpha_g \geqslant \alpha_{gc}: \quad \alpha^*_g = \alpha_g, \\ \alpha_g < \alpha_{gc}: \quad \alpha^*_g = \alpha_{gc}, \end{cases}$$

where c_{l0} is the sound velocity in the hexane-based magnetic fluid at the initial state ($c_{l0} = 1050.0$ m/s), and α_{gc} denotes the threshold of the void fraction ($\alpha_{gc} = 0.005$) [27].

The constitutive equation for gas-phase generation density (Γ_g) is as follows:

$$\Gamma_g = \Gamma_{ge} - \Gamma_{gc}, \tag{23}$$

where Γ_{ge} and Γ_{gc} denote the gas-phase evaporation density and gas-phase condensation density, respectively. By introducing constitutive equations for Γ_{ge} and Γ_{gc} to consider the effect of the surface tension (γ_l) in the cavitation inception process, we extend the classical nucleation theory for water droplets from subcooled vapor to hexane-based magnetic fluid. Namely, Γ_{ge} and Γ_{gc} are assumed to be proportional to the degree of subcooling and superheat. Furthermore, if Γ_{gk} ($k = e, c$) is expressed by the sum of the nucleation rate of the evaporated bubbles or the condensed liquid droplets as well as expressed by the increase in mass due to the growth of vapor bubbles and condensed droplets, the following equations for Γ_{gk} are derived [28,15]:

$$\Gamma_{gk} = \frac{4}{3}\pi\rho_k I_k R_{k(cr)}^3 + 4\pi\rho_k \sum_{i=1}^{i_{max}} N_{ki} R_{ki}^2 \frac{dR_{ki}}{dt}, \tag{24}$$

$$\begin{cases} I_k = \dfrac{A_c}{1+\Theta}\left(\dfrac{2\gamma_l}{\pi m_a^3}\right)^{1/2}\dfrac{\rho_g^2}{\rho_l}\exp\left(-\dfrac{4\pi R_{k(cr)}^2\gamma_l}{3k_B T_k}\right), \\ \Theta = \dfrac{2(\kappa_g - 1)}{\kappa_g + 1}\dfrac{\Delta h}{\Re T_g}\left(\dfrac{\Delta h}{\Re T_g} - 0.5\right), \\ R_{k(cr)} \approx \dfrac{2\gamma_l T_s}{\rho_k \Delta h \Delta T}. \end{cases}$$

In Eq. (24), subscript k has the same definition as that used in Eq. (16), R_k is the radius of a bubble or droplet, $R_{k(cr)}$ is the Kelvin–Helmholtz critical nucleate radius, k_B is Boltzmann's constant, I_k is the nuclei generation rate of vapor bubbles or liquid droplets, A_c is the condensation coefficient, Θ is the nonisothermal correction factor, m_a is the mass of a single molecule of hexane, γ is the surface tension, $\Re$ is the gas constant, T_s is the saturation temperature, and subscript i is the value at each calculation cell. Δh denotes the latent heat, which is described by the difference in specific enthalpy between the liquid and gas phases, and is defined as $\Delta h = h_l - h_g$. The temperature difference between saturation temperature and gas- or liquid-phase temperature, ΔT, is defined as $\Delta T = |T_s - T_k|$. N_{ki} denotes the number density of the generated vapor bubbles or condensed liquid droplets at each calculation cell (i).

By introducing the formulation of the growth process for bubbles and condensed droplets, we assume that the growth rate of a bubble or droplet is controlled by the rate at which the enthalpy of vaporization or condensation can be conducted away from the bubble and droplet to the bulk liquid [29]. Under that assumption, the equation of the growth process for a single vapor bubble and a condensed droplet is derived as

$$\Delta h \rho_k \frac{dR_{ki}}{dt} = \frac{p_k}{\sqrt{2\pi\Re T_g}}\frac{\kappa_k + 1}{2\kappa_k} c_{pk}\Delta T^{(i)}, \tag{25}$$

where $\Delta T^{(i)}$ denotes the interfacial temperature between the vapor phase and the condensed droplet and is derived by the following equation:

$$\Delta T^{(i)} = \left(1 - \frac{R_{k(cr)}}{R_{ki}}\right)|T_s - T_k|. \tag{26}$$

2.3. Numerical conditions and procedure

As a practical example, we use the fluid properties of a hexane-based temperature-sensitive magnetic fluid with manganese–zinc ferrite particles of 50% weight concentration [2]. The strength of magnetization M is approximated by the previous measurement data [2] and is expressed as a function of temperature T_l and the strength of magnetic field H as

$$\begin{cases} M = C_a \cdot f_1(H) \cdot f_2(T_l), \\ f(H) = 290.0 + 0.171H - 6.809\times10^{-7}H^2 + 1.007\times10^{-12}H^3 \\ \quad (H \leqslant 115.3\,\text{kA/m}), \\ f_2(T_l) = 6.675\times10^4 - 130.07T_l, \\ C_a = 3.108\times10^{-5}. \end{cases} \tag{27}$$

Next, in order to consider the effect of a nonuniform magnetic field as depicted in Fig. 2, the distributions of the longitudinal magnetic field component H^η and the transverse magnetic field component H^ξ are derived by the following equations. In introducing H^η and H^ξ, we referred to the analytical solution of the nonuniform magnetic field distribution of a Helmholtz coil [30] and the measurement results of the magnetic field of an electromagnet, which were used in the previous experimental studies [1,2]:

$$\begin{cases} H^\eta = H_{max} \cdot \exp(-\eta_h^{*2}), \\ H^\xi = H_{max} \cdot \xi^* \cdot |\eta_h^*| \cdot \exp(-\eta_h^{*2}), \\ \eta_h^* = \eta^* - \frac{1}{2}\eta_{max}^*, \end{cases} \tag{28}$$

where H_{max} is the maximum magnetic field strength; η^* denotes the normalized longitudinal coordinate, which is defined as $\eta^* = \eta/\eta_{max}$; and ξ^* denotes the normalized transverse coordinate, which is defined as $\xi^* = \xi/\xi_{max}$. The H_{max} on the electromagnet is installed in the nozzle throat.

The finite difference method is used to solve the set of governing equations mentioned above. In the present calculation, the discrete forms of these equations are semi-implicitly obtained using a staggered grid. The grid is concentrated at the nozzle wall to capture the cavitation inception precisely. The coordinate is transformed to the axisymmetric two-dimensional coordinate system and computation is performed in that coordinate system. The shape of bubble is assumed to be spherical.

The convective terms are discretized with a third-order QUICK scheme [31]. Also, the implicit fractional-step method [32] is used for time integration. Then the modified SOLA (numerical SOLution Algorithm for transient fluid

flow) method of Tomiyama et al. [19,33], which is superior for the formulation and solution of a gas liquid two-phase flow problem, is applied for the numerical calculation. The liquid-phase velocity, u_l^i, at the location of bubbles is calculated using an area-weighting interpolation method which was employed in the SMAC algorithm by Amsden and Harlow [34].

A free-slip condition for the prescribed liquid-phase velocity is applied to the central axis D–A, and the nonslip condition for prescribed liquid-phase velocity is applied to the sidewall C–B in Fig. 2. The inlet pressure and outlet pressure is applied in the initial stationary state. Immediately after the first time step computation is performed, the cross-sectional mean velocity with parabolic flow profile is computed and is subsequently employed as the inlet velocity profile. Therefore, a fully developed parabolic velocity profile is continuously applied for liquid-phase velocities to the inlet cross-sectional area of the flow duct A–B. A convective outflow condition is applied for liquid-phase velocities to the exit section of the duct D–C. Adiabatic conditions are applied for thermal boundary conditions at the duct-wall surface. The initial stationary condition of the liquid phase is assumed to be the pressurized fluid state.

The conditions for numerical analysis are listed in Table 1. For other physical properties used in constitutive equations, β_l and λ_l are given as a function of temperature and are defined by following empirical formula:

$$\begin{cases} \beta_l = \rho_l(2.247\times10^{-4} - 1.976\times10^{-6}T_l + 5.897\times10^{-9}T_l^2 \\ \qquad -5.926\times10^{-12}T_l^3)\ \text{(Pa s)}, \\ \lambda_l = 0.1412 + 3.4659\times10^{-4}T_l - 2.086\times10^{-6}T_l^2 \\ \qquad +2.431\times10^{-9}T_l^3\ \text{[W/(m K)]}. \end{cases} \tag{29}$$

The saturation temperature T_s is given as a function of pressure. The other required physical properties of the liquid phase are given by the tables of the thermophysical properties of hexane [35].

The interval of each time step is automatically adjusted during the computation to satisfy the CFL condition [18,33]. We actually calculated solutions on three different grid densities: 50×120, 60×150, and 100×220 nodes. As a result, we found that the each numerical result shows almost the same profile, and thus the grid independence of the numerical results was confirmed. Therefore, as a compromise between computer memory and accuracy, we chose to use a 60×150 structured grid in the ξ and η directions for the calculations. During the execution of the unsteady calculation, no significant differences in the mean flow profiles were found in the 1200–1500 time steps. We determined that the cavitating flow almost reaches steady state when such flow profiles are obtained.

Table 1
Numerical conditions

Density	ρ_l	1386.0 kg/m^3
Inlet pressure	$p_{l(in)}$	0.20 MPa
Outlet pressure	$p_{l(ex)}$	0.101 MPa
Inlet temperature	$T_{l(in)}$	283 K
Inlet internal energy	$e_{l(in)}$	1205.0 kJ/kg
Surface tension	γ_l	0.0213 N/m
Inner width of duct	D	8.0 mm

In addition, in order to clarify the effects of magnetic field and Reynolds number Re on the generation of cavitation, the cavitation number σ is introduced as follows [36]:

$$\sigma = \frac{p_{l(th)} - p_s}{\frac{1}{2}\rho_l \overline{u_{l(th)}^i}^2}, \tag{30}$$

$$Re = \frac{|\overline{u_{l(th)}^i}|\cdot d}{\nu_l}, \tag{31}$$

where $p_{l(th)}$ is the static pressure at the nozzle throat, p_s is the saturated vapor pressure, d is the nozzle throat width, $u_{l(th)}^i$ is the liquid-phase velocity vector at the nozzle throat, and the overline — denotes the cross-sectional mean value.

3. Results and discussion

Fig. 3 shows the numerical results of the transient evolution of the void fraction (α_g) contour, and Fig. 4 shows the instantaneous liquid-phase pressure (p_l) contour. According to Fig. 3, cavitation inception effectively occurs in the divergent nozzle throat. In the case of a strong magnetic field [$H_{max} = 115.3$ kA/m, Case (a)], cavitation formation of a cloud cavity at the diverging nozzle throat is more greatly suppressed than that of a nonmagnetic field [$H_{max} = 0$ kA/m, Case (b)] due to the magnetic body force under a sharp magnetic field gradient. The growth rate of the volume fraction of the cavitation bubble in the strong magnetic field is found to be smaller than that in the nonmagnetic field. Focusing on Case (a), immediately after the flow is initially induced, taking note of the primary feature of the void fraction profile under a strong magnetic field, the void fraction profile becomes elongated in the longitudinal direction of negative magnetic field gradient because the bubbles are accelerated and migrate due to the two-phase magnetic body force in the direction of the negative magnetic field gradient. The effect of two-phase magnetic body force is characterized by the second right-hand term in the momentum equation (Eq. 2).

With the elapse of time, because the magnetic body force based on the transverse magnetic field gradient acts so that the bubbles migrate from the wall into the center of the duct, it becomes clear that the void fraction increases locally near the central axis. Downstream of the nozzle throat, although magnetic body force acts as flow resistance, the forces decreases due to the gas-phase inclusion. In the two-phase flow region, not only the decreasing effect of flow resistance due to the negative magnetic field gradient, but also the pressure-rise effect caused by the unbalance of the magnetic body force between the single- and two-phase flow region are obtained.

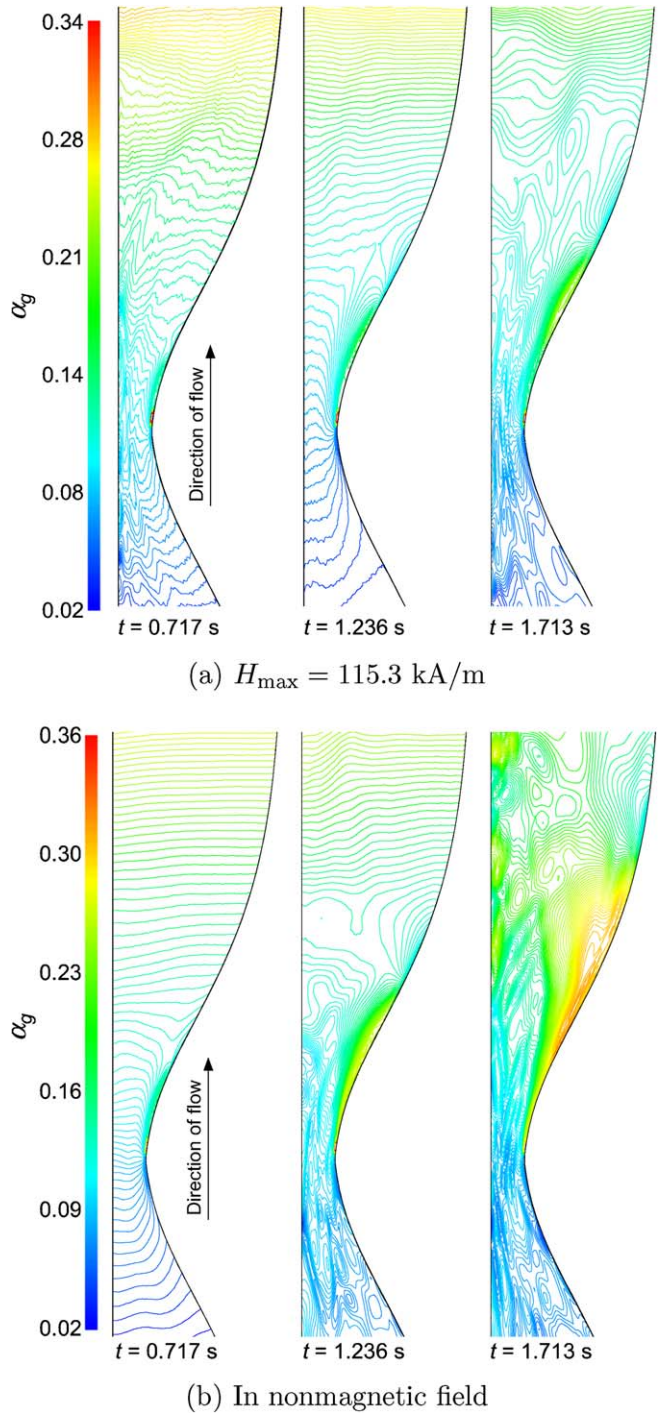

Fig. 3. Effect of nonuniform magnetic field on time evolution of void fraction distributions (enlarged view of nozzle throat section).

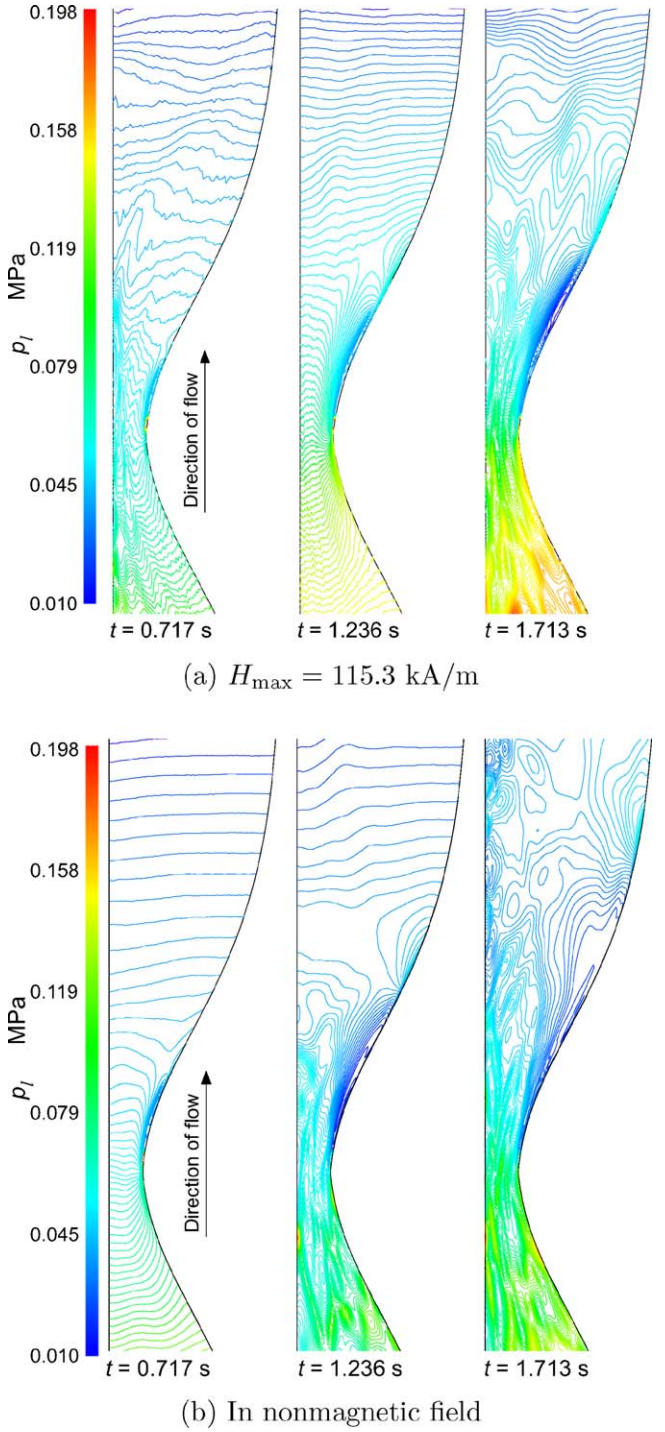

Fig. 4. Effect of nonuniform magnetic field on instantaneous liquid-phase pressure contours (enlarged view of nozzle throat section).

Furthermore, additional lift force operates in the transverse direction, which causes the bubbles to migrate in the duct-wall direction. However, as the two-phase magnetic body force begins to dominate the bubbles, it is found that the large volume fraction region of gas phase moves to the central axis of the duct. According to this result, the gas-phase motion is controlled not only by the buoyancy force, but also by the liquid-phase pressure gradient, additional lift forces, and especially by the two-phase magnetic body force that acts on the cavitation bubbles.

If the phenomenon applicable to the conditions of both a strong magnetic field and nonmagnetic field is as explained here, then the gas-phase volume fraction increases at the throat position and is concentrated to form a small cavity cloud downstream of the divergent nozzle due to the small vortex induced by the wake passing

through the nozzle throat, which is due to the effect of the negative pressure gradient. When the magnitude of the cloud cavity is above a certain size, due to the re-entrant jet resulting from the boundary layer separation, the cavity becomes detached from the cloud and then remains in the high-volume fraction region as the gas phase moves downstream. Especially in the case of a strong magnetic field, because the two-phase magnetic ejection effect acts on the cloud cavity in the negative magnetic field gradient region, the separation of the cloud cavity is enhanced by the two-phase magnetic body force acting on the cavitation bubbles. Due to the effects of suppression and magnetic ejection on the cavitation bubbles as well as the enhancement of the cloud cavity separation, the magnitude of the cloud cavity under a strong magnetic field becomes smaller than that of a nonmagnetic field, and a more homogeneous two-phase flow is generated under the strong magnetic field than that in the case of the nonmagnetic field.

Fig. 5 shows the present numerical results of the effect of the liquid-phase pressure rise in the longitudinal direction, in comparison with the previous one-dimensional numerical result for its effect in the steady boiling two-phase pipe flow of magnetic fluid and with the experimental results of the pressure-rise effect in the longitudinal direction for the steady boiling two-phase pipe flow and injected gas–liquid two-phase pipe flow of magnetic fluid [2]. In this figure, the axis of the ordinate denotes the normalized pressure-rise parameter (Δp_l^*) and is derived by the following equation:

$$\Delta p_l^* = \frac{\overline{p_{l(\mathrm{eff})}} - p_{l(\mathrm{in})}}{p_{l(\mathrm{in})}}, \tag{32}$$

where $\overline{p_{l(\mathrm{eff})}}$ is the cross-sectional mean-effective driving pressure from which the influence on the prudence of the liquid-phase fluid can be deducted. $p_{l(\mathrm{in})}$ is the inlet pressure. The axis of the abscissa in Fig. 5 denotes the normalized longitudinal coordinate $\eta^*(=\eta/\eta_{\max})$. Focusing on the present numerical result of cavitating magnetic fluid flow, the pressure-rise effect based on the two-phase magnetic body force under an applied magnetic field region acts effectively at the initial stage of cavitating flow in the two-phase downstream region. However, as time elapses and the flow approaches steady state, the pressure-rise effect, which is based on cavitating two-phase magnetic body force is found to decrease especially around the exit section of the duct.

Comparing our previous results regarding the pressure distribution of the boiling two-phase and injected gas–liquid two-phase magnetic fluid flow [2] with the present numerical results, it is found that the present fluid acceleration system which uses cavitation can achieve a greater pressure-rise effect. Also, it is found that a greater pressure-rise effect can be obtained by those kinds of two-phase production method in the following order: 1. cavitating flow > 2. boiling two-phase flow > 3. injected gas–liquid two-phase flow of magnetic fluids. Therefore, when a fluid driving system which uses two-phase magnetic fluid is employed, a rather high pressure-rise effect resulting from the use of cavitation for two-phase flow production can be obtained.

Fig. 6 shows the fluctuation of bubble radius (R_g) as a function of the time at position E (as depicted in Fig. 2, $\eta = 0.5\eta_{\max}$), which is just a quarter of the nozzle throat width, where the cavitation actively occurs. It is found that the magnitude of transient displacement of R_g in the case of a strong magnetic field ($H_{\max} = 115.3$ kA/m) has a smaller value and that the size of R_g becomes more homogeneous than that in the case of a nonmagnetic field because the

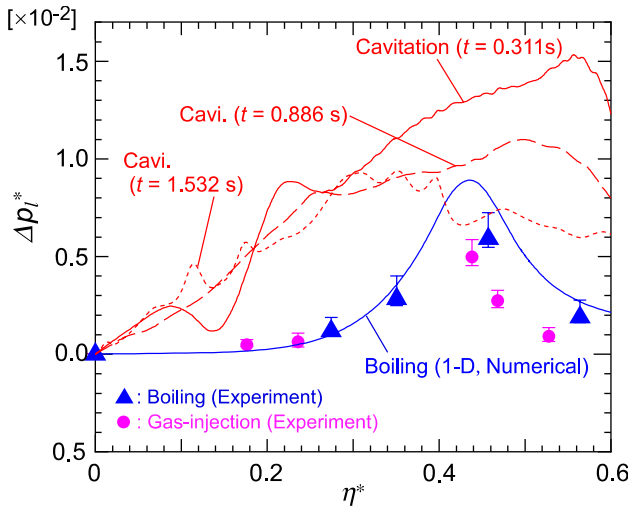

Fig. 5. Normalized pressure-rise effect Δp_l^* in cavitating flow of magnetic fluid along the central axis A–D, in comparison with the previous one-dimensional numerical result and experimental results of Δp_l^* along the longitudinal direction for steady boiling two-phase and gas–liquid two-phase pipe flow of magnetic fluid [2].

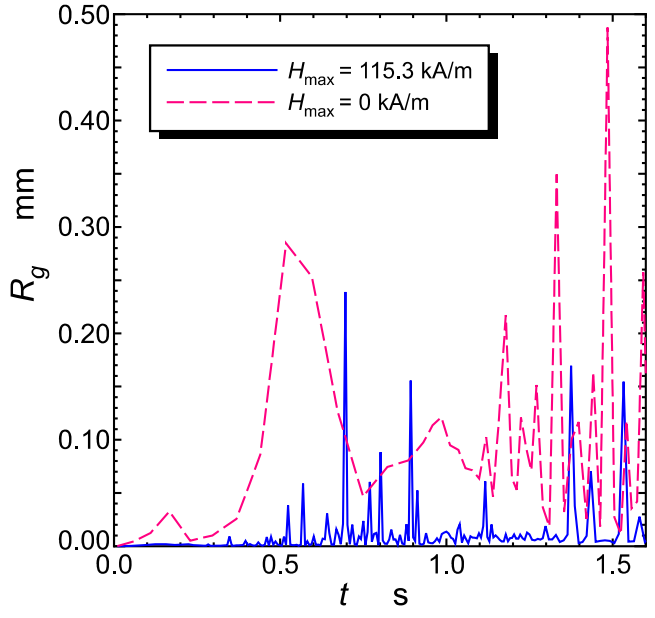

Fig. 6. Effect of nonuniform magnetic field on fluctuations of bubble radius as a function of time.

magnetic body force acts to suppress the expanding cavitation bubbles. From Figs. 3–6, it is clarified that the decrease of p_l induces an increase of α_g and that the expansion or contraction of bubble radius R_g corresponds to the change of p_l. Since the displacement magnitude of R_g has a small value, it is also clarified that the generated cavitation bubbles maintain a small size in the vaporization process and in the initial cavitating flow state.

Fig. 7 shows the effect of magnetic acceleration on the longitudinal liquid-phase cross-sectional mean velocity, $\overline{u_l^\eta}$, as a function of time (t). In the case of a strong magnetic field (a), the fluid acceleration effect which is based on the two-phase magnetic body force, increases with the lapse of time. It is found that $\overline{u_l^\eta}$ sharply increases in the flow field and becomes a two-phase flow state, especially increasing at the converging section of the nozzle throat ($\eta = 0.5\eta_{max}$), and that $\overline{u_l^\eta}$ tends to express the maximum value at the exit section of the duct. In the case of the nonmagnetic field (b), it is found that $\overline{u_l^\eta}$ increases with an increase in time (t). However, the magnitude of $\overline{u_l^\eta}$ exhibits a lower value than that of $\overline{u_l^\eta}$ in the case of a strong magnetic field. Furthermore, it is found that the rate of increase on $\overline{u_l^\eta}$ in a strong magnetic field shows a greater value than that in a nonmagnetic field. It is also found that the fluctuation of $\overline{u_l^\eta}$ in the vicinity of the outlet section sharply increases with maximum time step because of the rapid propagation of the velocity and pressure fluctuations from the nozzle throat section to the outlet section of the duct. The pressure fluctuation at the nozzle throat is caused by the effects of sudden cavitation generation and rapid bubble growth with time, also by the high-speed inflow of liquid phase into the throat section. The magnitude of velocity sharpness does not so vary or increase any more when the flow state becomes to the steady state.

Fig. 8 shows the profiles of the liquid-phase velocity (u_l^i) around the throat section. The flow separation and backward flow of u_l^i locally occur in the vicinity of the wall of the throat section upstream of the point of cavitation inception. In the case of a strong magnetic field ($H_{max} = 115.3$ kA/m), the liquid phase is locally accelerated around the throat wall section and the magnitude of u_l^i has a larger value compared with the case of a nonmagnetic field because of the two-phase magnetic acceleration effect which acts on the liquid phase due to the strong magnetic field gradient. In the throat wall vicinity where cavitation is actively generated, the liquid-phase velocity is strongly accelerated because of the two-phase magnetic driving force and the effect of bubbles pumping acting on the liquid phase. The slip ratio (u_g^i/u_l^i) in the vicinity of throat wall section tends to have a large value. Furthermore, because of the increase in momentum exchange between the gas and liquid phases, the magnitude of u_l^i locally increases in the region where the cavitation is actively generated. According to the results, it is found that rather than utilizing only the pumping effect of the bubbles when employing the two-phase fluid driving system, the method which utilizes the two-phase magnetic body force

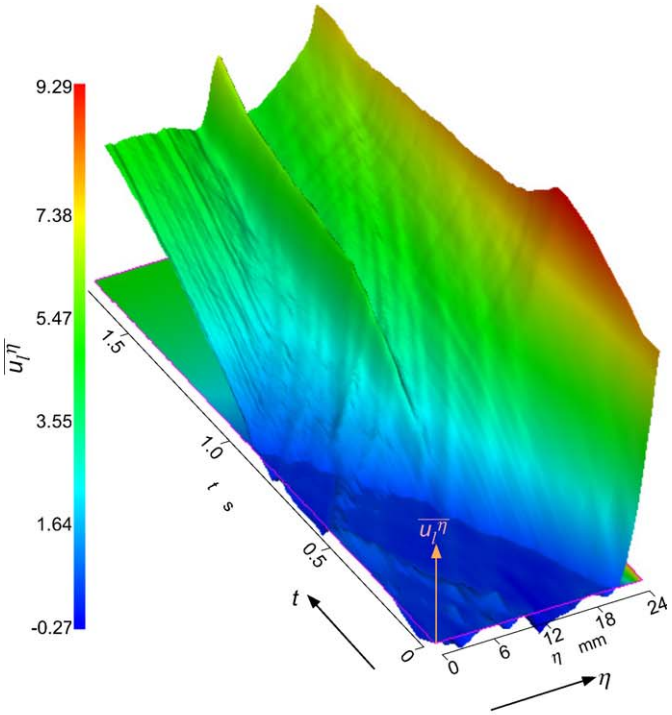

(a) $H_{max} = 115.3$ kA/m

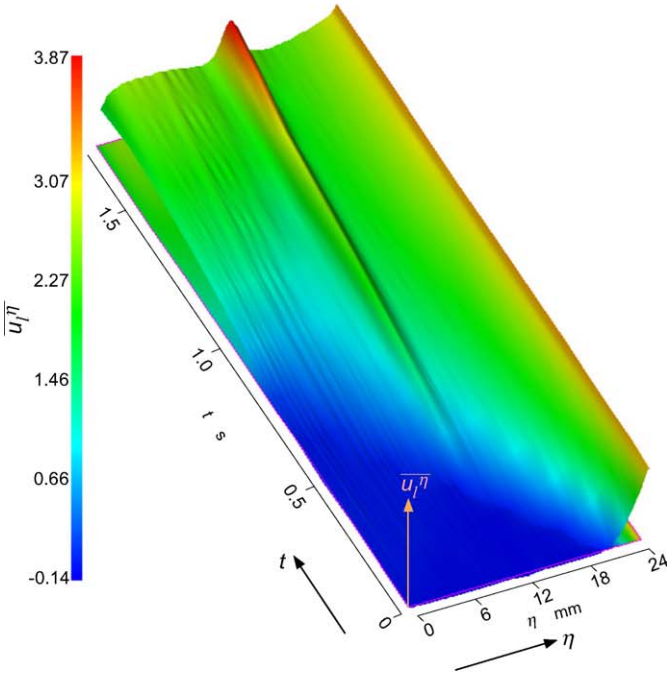

(b) In nonmagnetic field

Fig. 7. Effect of magnetic acceleration on the longitudinal liquid-phase cross-sectional mean velocity as a function of time.

generated by cavitating magnetic fluid flow can obtain the enhanced fluid acceleration effect.

Fig. 9 shows the instantaneous gas-phase velocity u_g^i around the throat section. In the initial flow state, it is found that the backward flow of u_g^i is generated upstream of the throat due to the effect of the separation wake of

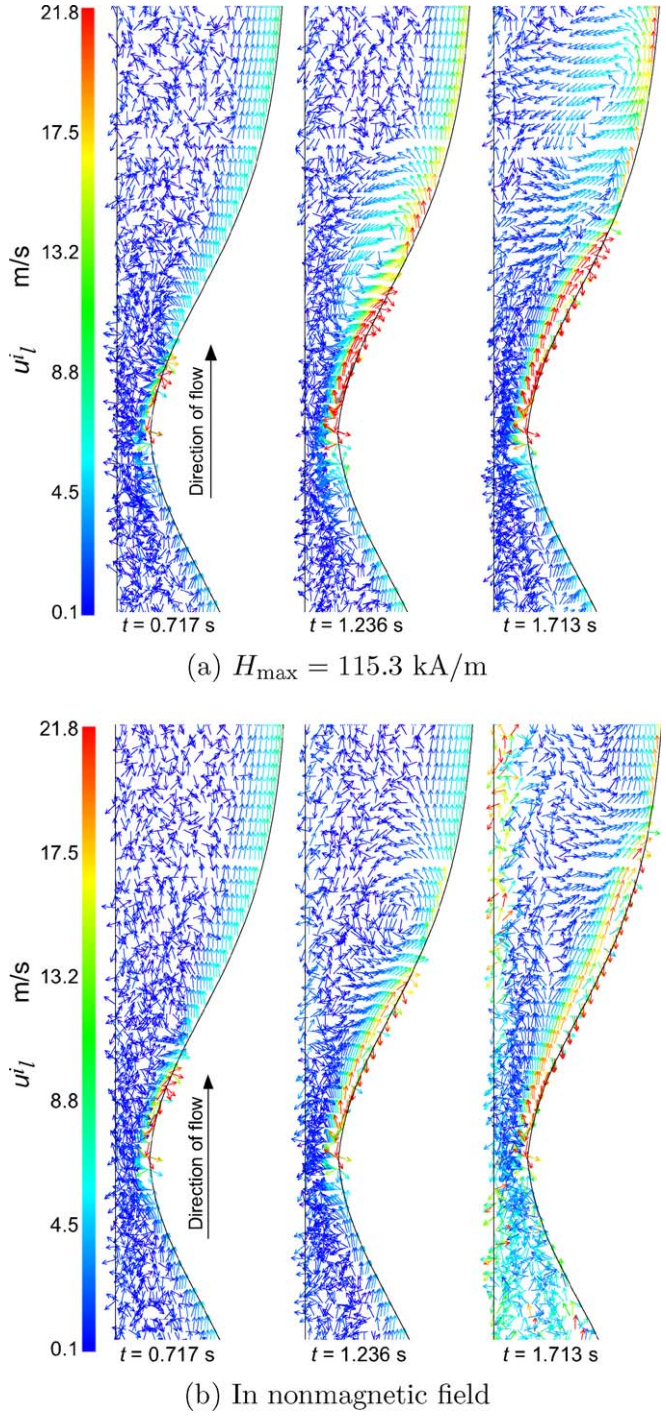

Fig. 8. Effect of nonuniform magnetic field on instantaneous liquid-phase velocity vector (enlarged view of nozzle throat section).

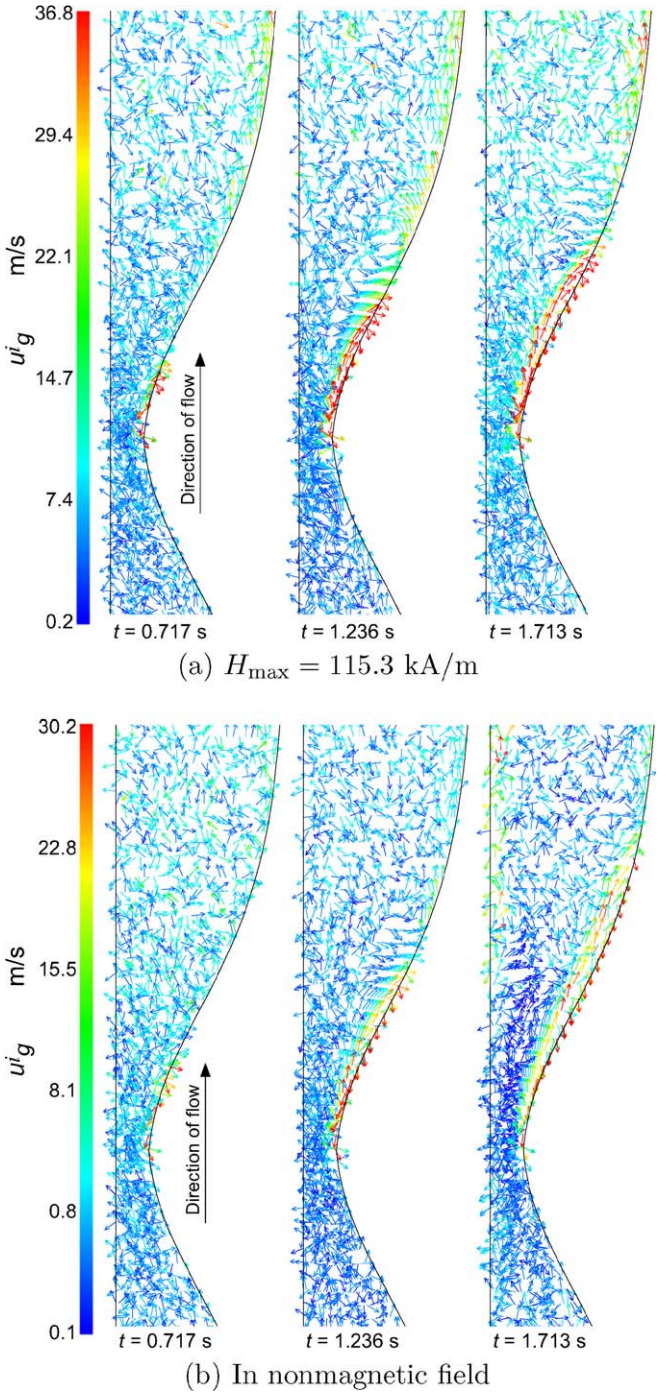

Fig. 9. Effect of nonuniform magnetic field on instantaneous gas-phase velocity vector (enlarged view of nozzle throat section).

liquid phase in the vicinity of the throat wall and that the gas phase is dispersed throughout the downstream region of the throat section. In the case of a strong magnetic field (a), the gas phase is locally accelerated in the direction of the negative magnetic field gradient, and the magnitude of u^i_g is indicated to have a larger value compared with the case of a nonmagnetic field (b) because of the magnetic ejection effect, which acts on the bubbles. Considering Figs. 9 and 3 together, in the strong magnetic field gradient region, the void fraction α_g locally decreases due to application of the nonuniform magnetic field because the gas phase is locally accelerated and the slip ratio increases due to the magnetic ejection effect on bubbles in the two-phase region.

In addition to the formation of the cavity vortex and its growth in the strong magnetic field, the advection of the cavity cloud is enhanced by the magnetic ejection effect in the downstream region of the throat. With time, the

gas-phase motion exhibits diffusing behavior, and the u_g^i profile takes on a different aspect from the liquid-phase velocity profiles (u_l^i). The characteristic gas-phase behavior in the magnetic fluid is not only due to the several additional forces that appear in Eq. (4), but also to the two-phase magnetic body force which acts on the bubbles that is included in the momentum terms in Eq. (2). According to the numerical results on gas-phase behavior, it is clarified that the precise control of bubble motion and control of the two-phase flow is possible by practical use of the characteristic magnetization of fluid inherent in magnetic fluid.

Fig. 10 shows the effect of magnetic field on cavitation number σ as a function of Reynolds number Re. The cavitation number σ is defined as Eq. 30. According to the numerical results, the profile of σ in the case of a strong magnetic field is found to have a larger value than that in the case of a nonmagnetic field. The increase of σ with an increase in magnetic field strength is caused by the increase of magnetic body force acting on the liquid-phase static pressure at the nozzle throat ($p_{l(th)}$). Additionally, it is found that the effect of magnetic body force on the magnitude of σ is more dominant than the magnetic acceleration effect.

If the phenomenon applicable to the conditions of the case with and that without the magnetic field is as explained here, σ decreases with an increase in the Re in the region of small Reynolds number, and the profile of σ tends to lean to the left. This tendency is due to the small magnitude of whole static pressure at the same σ which arose due to the small liquid-phase velocity. Contrarily, σ increases with an increase in the Re in the region of high Reynolds number. Especially in the case of a strong magnetic field, it is found that the positive gradient of increasing σ tends to become large and tends to lean to the right in the region of high Reynolds number. Therefore, it may be said that magnetic control for suppression of cavitation bubbles is remarkably enhanced in the condition of high Reynolds number.

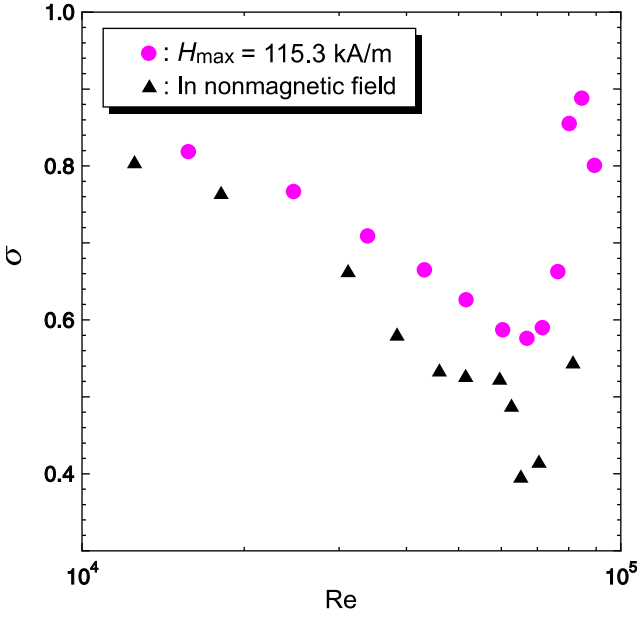

Fig. 10. Effect of magnetic field on cavitation number as a function of Reynolds number.

4. Conclusions

(1) Formation of a cloud cavity in the case of a strong magnetic field in the diverging nozzle throat is more greatly suppressed than such formation in the case of a nonmagnetic field due to a magnetic body force with a sharp magnetic field gradient. Especially in the case of a strong magnetic field, because the two-phase magnetic ejection effect acts on the cloud cavity in the negative magnetic field gradient region, separation of the cloud cavity is enhanced by the two-phase magnetic body force acting on the cavitation bubbles.

(2) The pressure-rise effect due to the two-phase magnetic body force under an applied magnetic field region effectively acts in the downstream two-phase region. The magnitude of the pressure-rise effect in the cavitating magnetic fluid flow has a larger value than the magnitude in the boiling two-phase magnetic fluid flow.

(3) Rather than utilizing only the pumping effect of bubbles when employing the two-phase fluid driving system, the method that utilizes the two-phase magnetic body force generated by cavitating magnetic fluid flow was found to be capable of obtaining an enhanced fluid acceleration effect.

(4) The cavitation number in the case of a strong magnetic field has a larger value than that in the case of a nonmagnetic field. Magnetic control for suppression of cavitation bubbles is remarkably enhanced in the condition of high Reynolds number.

Acknowledgements

The authors would like to thank Emeritus Prof. Shinichi Kamiyama and Prof. Hideya Nishiyama (Inst. Fluid Sci., Tohoku University, Japan) for their helpful discussions. This research was supported by a Grant-in-Aid for Scientific Research (C. No. 17686015) from the Ministry of Education, Science and Culture, Japan, and was also supported by TEPCO Research Foundation, Japan.

References

[1] J. Ishimoto, M. Okubo, H. Nishiyama, S. Kamiyama, Basic study on an energy conversion system using gas–liquid two-phase flows of magnetic fluid (analysis on the mechanism of pressure rise), JSME Int. J. Ser. B 39 (1995) 72–79.

[2] S. Kamiyama, J. Ishimoto, Boiling two-phase flows of magnetic fluid in a nonuniform magnetic field, J. Magn. Magn. Mater. 149 (1995) 125–131.

[3] M. Petrick, H. Branover, Liquid metal MHD power generation—its evolution and status, Prog. Astro. Aero. 100 (1985) 371–400.

[4] S.W. Charles, J. Popplewell, Progress in the development of ferromagnetic liquids, IEEE Trans. Magn. MAG-16 (1980) 172–177.
[5] V.A. Alekseev, I.Y. Veprik, S.G. Minukov, A.I. Fedonenko, Influence of microstructure on physico-mechanical properties of liquid metal-based magnetic colloids, J. Magn. Magn. Mater. 85 (1990) 133–136.
[6] A.I. Fedonenko, V.I. Smirnov, Particle interaction and clumping an electrically conducting magnetic fluid, J. Magn. Magn. Mater. 19 (1983) 388–391.
[7] S. Hoon, J. Popplewell, S. Charles, The resistivity of conducting ferromagnetic liquids containing iron particles in mercury, IEEE Trans. Magn. 14 (5) (1978) 981–983.
[8] M. Okubo, J. Ishimoto, H. Nishiyama, S. Kamiyama, Analytical study on two-phase MHD flow of electrically conducting magnetic fluid, Magnetohydrodynamics 29 (1993) 291–297.
[9] S. Eckert, G. Gerbeth, O. Lielausis, The behaviour of gas bubbles in a turbulent liquid metal magnetohydrodynamic flow, Part I: dispersion in quasi-two-dimensional magnetohydrodynamic turbulence, Int. J. Multiphase Flow 26 (2000) 45–66.
[10] S. Eckert, G. Gerbeth, O. Lielausis, The behaviour of gas bubbles in a turbulent liquid metal magnetohydrodynamic flow, Part II: magnetic field influence on the slip ratio, Int. J. Multiphase Flow 26 (2000) 67–82.
[11] J. Ishimoto, M. Okubo, S. Kamiyama, Effect of magnetic field on the stability of boiling two-phase flows of magnetic fluid, in: Proc. 2nd Int. Conf. Multiphase Flow, vol. 4, 1995, pp. FC17–FC24.
[12] I. Kataoka, A. Serizawa, Basic equations of turbulence in gas–liquid two-phase flow, Int. J. Multiphase Flow 15 (1989) 843–855.
[13] F.H. Harlow, A.A. Amsden, Numerical calculation of multiphase fluid flow, J. Comput. Phys. 17 (1975) 19–52.
[14] S. Yamamoto, Preconditioning method for condensate fluid and solid coupling problems in general curvilinear coordinates, J. Comput. Phys. 207 (1) (2005) 240–260.
[15] J.B. Young, Two-dimensional, nonequilibrium, wet-stream calculations for nozzles and turbine cascades, Trans. ASME J. Turbomach. 114 (1992) 569–579.
[16] K. Ueno, T. Nishita, S. Kamiyama, Numerical simulation of deformed single bubbles rising in magnetic fluid, J. Magn. Magn. Mater. 201 (1999) 281–284.
[17] M.M. Cross, Viscosity–concentration–shear rate relations for suspensions, Rheol. Acta 14 (1975) 402–403.
[18] A. Tomiyama, M. Hirano, An improvement of the computational efficiency of the SOLA method, JSME Int. J. Ser. B 37 (1994) 821–826.
[19] A. Tomiyama, H. Tamai, I. Zun, S. Hosokawa, Transverse migration of single bubbles in simple shear flows, Chem. Eng. Sci. 57 (2002) 1849–1858.
[20] L.S. Fan, C. Zhu, Principles of Gas–Solid Flows, Cambridge University Press, New York, NY, 1998.
[21] N.A. Patankar, D.D. Joseph, Modeling and numerical simulation of particle flows by the Eulerian–Lagrangian approach, Int. J. Multiphase Flow 27 (2001) 1659–1684.
[22] Y. Murai, Y. Matsumoto, Numerical study of the three-dimensional structure of a bubble plume, Trans. ASME J. Fluids Eng. 122 (2000) 754–760.
[23] T.R. Auton, The force exerted on a body in invisid unsteady non-uniform rotational flow, J. Fluid Mech. 197 (1988) 241–257.
[24] R. Clift, J.R. Grace, M.E. Weber, Bubbles, Drops, and Particles, Academic Press, San Diego, CA, 1978.
[25] F. Dobran, Liquid and gas-phase distributions in a jet with phase change, Trans. ASME J. Heat Transf. 110 (1988) 955–960.
[26] C.W. Solbrig, J.H. McFadden, R.W. Lyczkowski, E.D. Hughes, Heat transfer and friction correlations required to describe steam–water behavior in nuclear safety studies, AIChE Symp. Ser. 174 (1978) 100–128.
[27] C.W. Hirt, N.C. Romero, Application of a drift flux model to flashing in straight pipes, LA-6005-MS, Los Alamos Scientific Laboratory Report, 1975.
[28] S. Yamamoto, H. Hagari, M. Murayama, Numerical simulation of condensation around the 3-D wing, Trans. Jpn. Soc. Aero. Space Sci. 138 (1997) 182–189.
[29] C.A. Moses, G.D. Stein, On the growth of steam droplets formed in laval nozzle using both static pressure and light scattering measurements, Trans. ASME J. Fluids Eng. 100 (1978) 311–322.
[30] D.R. Otis, Computation and measurement of Hall potentials and flow-field perturbations in magnetogasdynamic flow of an axisymmetric free jet, J. Fluid Mech. 24 (1966) 41–63.
[31] B.P. Leonard, A stable and accurate convection modelling procedure based on quadratic upstream interpolation, Comput. Meth. Appl. Mech. Eng. 19 (1979) 59–98.
[32] M. Rosenfeld, D. Kwak, M. Vinokur, A fractional step solution method for the unsteady incompressible Navier–Stokes equations in generalized coordinate systems, J. Comput. Phys. 94 (1991) 102–137.
[33] A. Tomiyama, N. Shimada, A numerical method for bubbly flow simulation based on a multi-fluid model, Trans. ASME J. Pressure Vessel Tech. 123 (2001) 510–516.
[34] A.A. Amsden, F.H. Harlow, The SMAC method: a numerical technique for calculating incompressible fluid flows, LA-4370, Los Alamos Scientific Laboratory Report, 1970.
[35] JSME, Thermophysical Properties of Fluids, The Japan Society of Mechanical Engineers, Tokyo, 1997.
[36] K. Sato, Y. Saito, Unstable cavitation behavior in a circular–cylindrical orifice flow, JSME Int. J. Ser. B 45 (3) (2001) 638–645.